An Experimental and Theoretical Analysis of Ultrasound-Induced Permeabilization of Cell Membranes

Jagannathan Sundaram, Berlyn R. Mellein, and Samir Mitragotri
Department of Chemical Engineering, University of California, Santa Barbara, California 93106

ABSTRACT Application of ultrasound transiently permeabilizes cell membranes and offers a nonchemical, nonviral, and noninvasive method for cellular drug delivery. Although the ability of ultrasound to increase transmembrane transport has been well demonstrated, a systematic dependence of transport on ultrasound parameters is not known. This study examined cell viability and cellular uptake of calcein using 3T3 mouse cell suspension as a model system. Cells were exposed to varying acoustic energy doses at four different frequencies in the low frequency regime (20–100 kHz). At all frequencies, cell viability decreased with increasing acoustic energy dose, while the fraction of cells exhibiting uptake of calcein showed a maximum at an intermediate energy dose. Acoustic spectra under various ultrasound conditions were also collected and assessed for the magnitude of broadband noise and subharmonic peaks. While the cell viability and transport data did not show any correlation with subharmonic ($f/2$) emission, they correlated with the broadband noise, suggesting a dominant contribution of transient cavitation. A theoretical model was developed to relate reversible and irreversible membrane permeabilization to the number of transient cavitation events. The model showed that nearly every stage of transient cavitation, including bubble expansion, collapse, and subsequent shock waves may contribute to membrane permeabilization. For each mechanism, the volume around the bubble within which bubbles induce reversible and irreversible membrane permeabilization was determined. Predictions of the model are consistent with experimental data.

INTRODUCTION

One of the critical elements of medical therapy is effective and targeted delivery of drugs into cells and tissues. The lipid bilayer of cell membranes poses the primary barrier to transport of low- as well as high-molecular weight molecules into cells (Stein, 1986). Among the methods proposed to enhance cellular drug delivery are biological approaches including viruses for gene therapy (Johnson-Saliba and Jans, 2001), physical methods including electroporation (Canatella and Prausnitz, 2001), chemical methods such as cationic lipids (Brown et al., 2001), and drug conjugates (Fischer et al., 2001). Another approach to enhancing cellular drug delivery involves the use of ultrasound to transiently disrupt cell membranes.

The primary advantage of ultrasound is that as a physical, rather than a chemical approach, the enhancement is likely to be broadly applicable to a variety of drugs and cell types. Furthermore, based on the available methodologies to focus ultrasound in the body (Kremkau, 1998), ultrasound-mediated drug delivery may be targeted to designated regions. Ultrasound-enhanced delivery into cells has been demonstrated in vitro by uptake of extracellular fluid, drugs, and DNA into cells (Bao et al., 1997; Fecheimer et al., 1987; Guzman et al., 2001; Kim et al., 1996; Koch et al., 2000; Miller and Quddus, 2000; Miller et al., 1996, 1998; Saad and Hahn, 1992; Ward and Wu, 1999; Ward et al., 2000; Williams, 1973; Wu et al., 2002) and plant tissues (Zhang et al., 1991). Although exciting applications of ultrasound in drug delivery have been demonstrated, there is limited information available to guide the selection of optimal ultrasound conditions and even less information is available on the mechanism by which ultrasound achieves membrane permeabilization.

Effect of ultrasound on cell membrane permeability has been investigated under a variety of intensities (or pressure amplitudes) and frequencies (Bao et al., 1997; Guzman et al., 2001; Ward et al., 2000). However, a systematic investigation of the dependence of transport on ultrasound frequency and intensity is yet to be done. This is one of the objectives of this study.

Ultrasound-mediated bioeffects are generally believed to be caused by cavitation (Miller et al., 1996). Acoustic cavitation involves the creation and oscillation of gas bubbles in a liquid (Leighton, 1997). Cavitation bubbles may exhibit sustained growth and oscillations over several acoustic cycles (stable cavitation) or violent growth and collapse in less than a cycle (transient or inertial cavitation) (Leighton, 1997). Potentially, both stable and transient cavitation may induce membrane permeabilization. Liu et al. (1998) reported that disruption of red blood cell membranes by ultrasound correlates better with the occurrence of stable cavitation. On the other hand, other investigators (Everbach et al., 1997; Miller et al., 1996) postulated that ultrasound-induced cell damage results from inertial (transient) cavitation. However, a systematic dependence of membrane permeabilization on ultrasound or cavitation parameters is not yet known.

Since bio-effects related to acoustic cavitation are inversely related to ultrasound frequency (Mitragotri et al., 1995; Tezel et al., 2001), low-frequency ultrasound should be more

Submitted October 1, 2002, and accepted for publication December 26, 2002.

Address reprint requests to Samir Mitragotri, Dept. of Chemical Engineering, University of California, Santa Barbara, CA 93106. Tel.: 805-893-7532; Fax: 805-893-4731; E-mail: samir@engineering.ucsb.edu.

© 2003 by the Biophysical Society

0006-3495/03/05/3087/15 $2.00

effective in enhancing membrane permeability. Accordingly, we designed a study focused on assessing the dependence of membrane permeabilization in low-frequency regime (20 kHz–100 kHz). In addition, we also performed acoustic spectroscopy to determine two cavitation-related parameters (subharmonic peak amplitude indicative of violent stable cavitation and broadband noise indicative of transient bubble collapse). A theoretical model to describe cavitation-mediated membrane permeabilization is also presented.

MATERIALS AND METHODS

Cell preparation

Effect of low-frequency ultrasound on membrane permeabilization was assessed using 3T3 mouse cells (ATCC, Manassas, VA). Cells were cultured as a monolayer in a humidified atmosphere with 95% air and 5% CO_2 at 37°C in Dulbecco's modified Eagle's medium (Sigma-Aldrich, St. Louis, MO) with 10% fetal bovine serum and 100 μg/ml penicillin-streptomycin. Cells were harvested before each experiment with versene followed by digestion using trypsin/EDTA (Cellgro, Herndon, VA). Cells were washed with DMEM medium and resuspended in Dulbecco's modified Eagle's medium in 12-well plates (Corning Inc., Corning, NY, well diameter of 2.3 cm) at concentrations varying between 7×10^5 cells/ml and 9×10^5 cells/ml. Two milliliters of cell suspension were used in each experiment.

Ultrasound application

Ultrasound was applied at four frequencies 20 kHz, 57 kHz, 76 kHz, and 93 kHz. For each frequency, a custom-built transducer was used to generate ultrasound (PiezoSystems Inc., Cambridge, MA). The transducers were designed by sandwiching ceramic crystals between two metal resonators of appropriate lengths. A signal generator (Tektronix CFG-280, Beaverton, OR) along with an amplifier (Krohn-Hite 7500, Avon, MA) was used to drive the transducers. The electric power applied to the transducer was measured using a sampling wattmeter (Clarke-Hess 2330, New York, NY). The frequency of the electrical signal was matched with the resonant frequency of each transducer. Transducers were calibrated using laser interferometry and hydrophone measurements using methods described by Tezel and co-workers (Tezel et al., 2001). The transducers were directly immersed in the cell suspension (Fig. 1 *A*). The tip of the transducer was located at the center of the well. The cross-sectional area of all transducers was 0.78 cm^2. A 100% duty cycle was chosen for ultrasound application.

Just before ultrasound application, a solution of a fluorescent dye, calcein (MW = 623 Da, Molecular Probes, Eugene, OR) was added to the wells. The amount of calcein was such that the final concentration of calcein in the well was 50 μM. Ultrasound was applied to each well for times in the range of 10–180 s. At the end of ultrasound application, transducer was removed from the well and the cell suspension was collected. Cells were centrifuged and washed several times with the medium to remove calcein from the extracellular space. These cells were then observed under a microscope to determine the fraction of cells into which calcein had penetrated. For this purpose, a 20 μl cell suspension was placed on a microscope slide and was imaged using a fluorescence microscope (Axiovert 25 Inverted Microscope, Zeiss). The images were captured under a constant exposure, illumination and gain (charge-coupled device camera, Optronics, Goleta, CA). These images usually showed a heterogeneous population.

To quantify the cells exhibiting transport, images of identical volumes of solutions containing various concentrations of calcein (0.5–50 μM in PBS) were captured under identical exposure and were compared to images of cells. Using these images, cells were classified into three categories: those exhibiting minimal transport (intracellular calcein concentrations between 0 and 0.5 μM; that is, between 0 and 1% of equilibrium concentration),

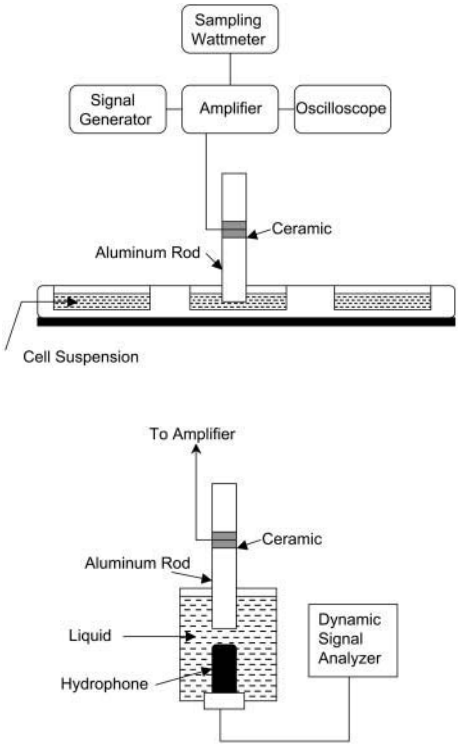

FIGURE 1 (*A*) A schematic representation of the setup used for ultrasound application to cell suspension. (*B*) A schematic representation of the setup used for acoustic spectroscopy.

moderate transport (intracellular calcein concentrations between 0.5 μM and 5 μM; that is, between 1 and 10% of equilibrium concentration), and high transport (intracellular calcein concentrations between 5 μM and 50 μM; that is, between 10 and 100% of equilibrium concentration). Although calcein standards were made in PBS and not in the cell cytoplasm, a comparison of calcein fluorescence in two media is feasible to a first approximation. The confidence in using PBS solution as a standard is supported by the observation that the fluorescence in the cell population exhibiting highest transport is comparable to that of a 50 μM calcein solution. Under an ultrasound condition where relatively high transport is observed (for example, 20 kHz, 0.8 W/cm^2, 30 s), ~38% of cells exhibited low transport, 27% cells exhibited moderate transport, and 8% cells exhibited high transport. The total number of cells exhibiting transport was thus 73%, while the remaining 27% cells were nonviable. For the purpose of quantifying transport, we report cells exhibiting high transport (intracellular calcein concentration in the range of 10–100% of equilibration). Under each ultrasound condition, at least 500–600 cells were counted to determine the fraction of cells exhibiting transport.

Under each ultrasound condition, viability of cells was also assessed using trypan blue. At the end of ultrasound exposure, cells were stained with trypan blue. These cells were observed under the microscope and the fraction of dead cells was counted. Each measurement was performed based on 20 μl of cell suspension.

Acoustic spectroscopy

Cavitation generated by ultrasound application was measured using acoustic spectroscopy. This method for monitoring cavitation involves the detection of bubble activity through measurement of the pressure spectrum of the acoustic field (Liu et al., 1998; Neppiras, 1968; Tezel et al., 2002). If the driving acoustic field is a continuous wave of frequency f, the acoustic pressure field scattered by the bubble contains special components of

harmonic frequency (2*f*, 3*f*, etc.), subharmonic frequency (for example, *f*/2) and ultraharmonic frequency (for example, 3*f*/2) (Neppiras, 1968; Shankar et al., 1999). At higher ultrasound intensities, transient cavitation is induced and results in the elevation of broadband noise. Measurements of subharmonic pressure amplitude as well as broadband noise were performed using a hydrophone (Model TC 4013, Reson, Goleta, CA). The bandwidth of the hydrophone is 1 Hz–170 kHz (−10 dB). The hydrophone diameter is 0.5 cm and the length is ~2 cm. The transducer diameter is 0.8 cm. Due to its large size, the hydrophone cannot be placed in the well. Accordingly, a separate chamber was used for measuring acoustic spectrum (Fig. 1 *B*). The diameter of this chamber was comparable to the well diameter, but the height was ~5 cm. The hydrophone was placed directly underneath the transducer and the chamber was filled with the cell culture medium. The transducer was completely immersed under the liquid. The output of the hydrophone was analyzed using a dynamic signal analyzer (Hewlett-Packard 3562A, Everett, WA). Detailed methods of measurements of acoustic spectrum are described by Tezel et al. (2002). Analysis of subharmonic emission in this article was performed using *f*/2 component. Peak amplitude of subharmonic component was measured by continuously averaging the acoustic spectrum until a steady value (within 10%) was reached. Broadband noise was measured over a frequency range of 1 Hz–100 kHz using the same hydrophone and method. The spectrum was averaged until a steady value (within 10%) was reached.

RESULTS AND DISCUSSION

Effect of low-frequency ultrasound on cell viability and calcein transport

Intracellular calcein concentration among the entire cell population after ultrasound application was heterogeneous and ranged from 0 to ~50 μM. Such heterogeneity of transmembrane transport upon ultrasound application is consistent with literature reports (Guzman et al., 2001; Kodama and Takayama, 1998). Investigation of the origin of the heterogeneity is beyond the scope of this article. To quantify transport data under such heterogeneous conditions, Guzman and co-workers divided the cell population into three categories, cells exhibiting minimal transport (~1% equilibration), cells exhibiting high transport (close to equilibration), and cells exhibiting intermediate transport (~10% equilibration) (Guzman et al., 2001). On the other hand, some investigators (Kodama et al., 2000) quantified transport in terms of fraction of cells exhibiting any detectable fluorescence.

In our study, as stated earlier, a large fraction of cells exhibited minimal transport (<1% of equilibration) and about the same fraction exhibited moderate transport (between 1% and 10% of equilibration). A small fraction exhibited high transport (intracellular concentration between 10 and 100% of equilibration). We performed quantitative data analysis based on this fraction of cells. Although this choice of intracellular concentration is somewhat arbitrary, we believe that the general conclusion of the dependence of transport on ultrasound parameters is insensitive to the choice of this threshold. With this choice of the threshold, the highest fraction of cells exhibiting transport under the range of ultrasound parameters explored was ~6–8%. A choice of a higher concentration threshold reduced the fraction of cells deemed permeable, thereby increasing the error in the analysis. On the other hand, a reduction of the threshold decreased the sensitivity of the dependence of transport on ultrasound parameters. Incorporation of concentration threshold in data analysis is discussed later in the manuscript. It is important to note that the cells exhibiting the presence of intracellular calcein correspond to the fraction of the cell population that was reversibly permeabilized. Calcein delivered into cells which were irreversibly permeabilized is removed during the washing procedure.

Fig. 2 *A* shows the variation of cell viability, V, with ultrasound energy density, E ($E = It$, where, I is ultrasound intensity in W/cm^2 and t is total application time in seconds) at four frequencies. The data at each frequency were obtained at a variety of intensities in the range of 0–3 W/cm^2 and application times in the range of 0–180 s. Scaling of bio-effects of ultrasound with total energy dose has been previously reported for ultrasound-mediated skin permeability and cell membrane permeabilization (Guzman et al., 2001; Mitragotri et al., 2000a,b; Tezel et al., 2001). Specifically, Tezel and co-workers reported that the effect of low-frequency ultrasound on skin permeability scales with the total energy density (Tezel et al., 2001). Similarly, Guzman et al. (2001) showed that the effect of ultrasound on cell membrane permeabilization also scaled with ultrasound energy density. This relationship between ultrasound-induced bio-effect and energy density facilitates the analysis since it allows for the combination of the dependence of bio-effect on three ultrasound parameters: intensity, application time, and duty cycle, into a single parameter—that is, energy density.

At each frequency, cell viability, V, decreased with increasing energy dose. The energy density at which viability drops below 50% is ~10 J/cm^2, 45 J/cm^2, 40 J/cm^2, and 60 J/cm^2, respectively at 20 kHz, 57 kHz, 76 kHz, and 93 kHz. The absolute values of these energy densities are likely to depend on various parameters including transducer geometry and liquid volume that were held constant in this study. Hence, relevance of the absolute values of these energy densities to membrane permeabilization should be carefully performed. However, the data clearly show that the energy density required for achieving low viability increases with increasing frequency.

Fig. 2 *B* shows the dependence of the fraction of cells exhibiting calcein uptake (that is, reversibly permeabilized, T) on ultrasound energy density at the same four frequencies. At each frequency, the fraction of fluorescent cells exhibited an optimum with respect to ultrasound energy. The highest fraction of cells exhibiting transport was between 6 and 8% for most frequencies. While this might represent a low level of transport efficiency, it has to be remembered that a high threshold was set for determining transport. Furthermore, the fraction of cells exhibiting transport may be further optimized.

The energy density corresponding to maximum calcein delivery increased with increasing frequency. For ultrasound at 20 kHz, 57 kHz, 76 kHz, and 93 kHz, the energy density corresponding to peak delivery was respectively 25 J/cm^2, 40 J/cm^2, 40 J/cm^2, and 75 J/cm^2. Once again, these energy

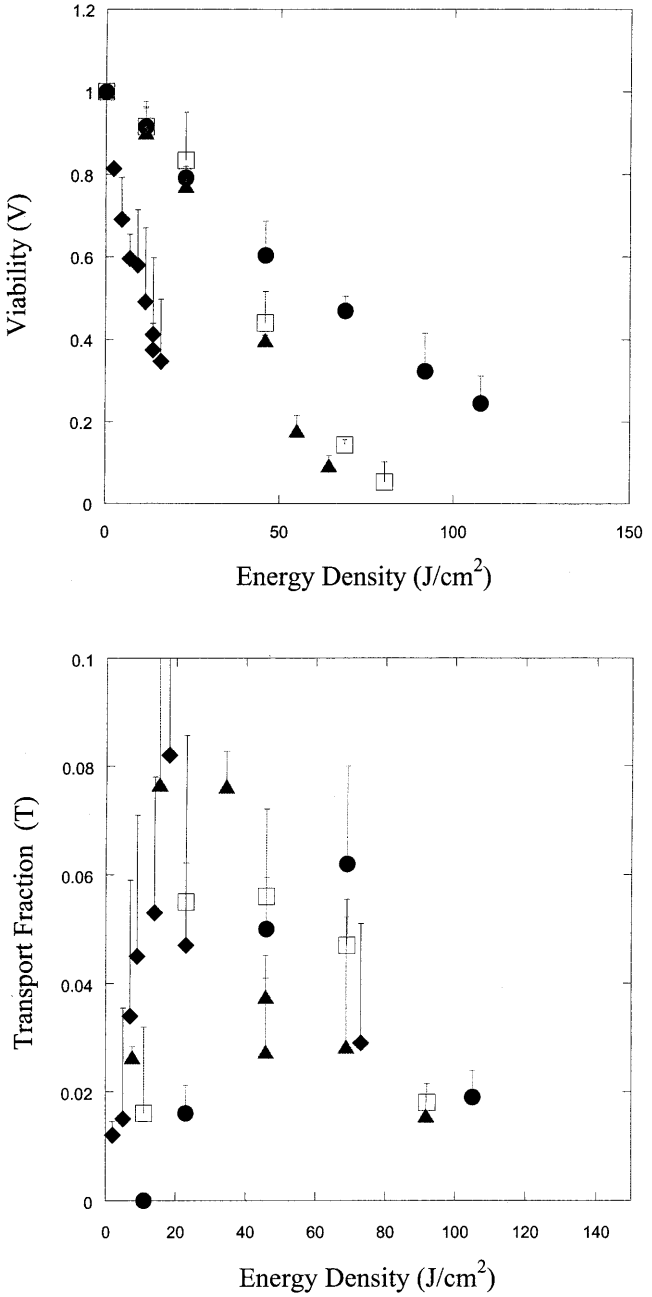

FIGURE 2 (*A*) Variation of cell viability (V) with ultrasound energy density at four frequencies (♦, 20 kHz; ▲, 57 kHz; □, 76 kHz; and ●, 93 kHz). Error bars show standard deviation on at least four repetitions. (*B*) Variation of cell population fraction exhibiting calcein transport (T) with ultrasound energy density at four frequencies (♦, 20 kHz; ▲, 57 kHz; □, 76 kHz; and ●, 93 kHz). Error bars show standard deviation on at least four repetitions.

values are likely to be system-specific. It is interesting that although the dependence of viability and intracellular calcein delivery on ultrasound energy density is clearly different for different frequencies, the maximum fraction of cells reversibly permeabilized (~6–8%) is nearly independent of the frequency. The absolute fraction of cells exhibiting transport will change if the threshold concentration is changed. However, the dependence of transport on ultrasound parameters will remain qualitatively the same (data not reported).

Dependence of viability and calcein transport on cavitation parameters

Acoustic cavitation has been shown to play an important role in several ultrasonically-mediated bio-transport problems (Liu et al., 1998; Miller et al., 1996; Mitragotri et al., 1995; Suslick, 1989). Cavitation manifests itself in at least two modes; stable cavitation (slow, periodic oscillations of gas bubbles) and transient cavitation (rapid, violent growth and collapse of gas bubbles; Suslick, 1989). The first step in identifying the detailed mechanisms of ultrasound-mediated membrane permeabilization is to identify which type of cavitation is responsible for this phenomenon. Cavitation generated by ultrasound application was measured using acoustic spectroscopy. Energy density associated with each type of cavitation (E_{bb} for broad band noise or E_{sh} for subharmonic emission) was determined using the equation, $E = (P^2/\rho c)t$, where P is the amplitude of subharmonic in case of stable cavitation (P_{sh}) in Pa and broadband noise (P_{bb}) in the case of transient cavitation and t is the ultrasound application time in seconds.

Fig. 3 shows the dependence of viability on transient cavitation energy for all four frequencies shown in Fig. 2 *A*. As expected, the cell viability decreases with increasing

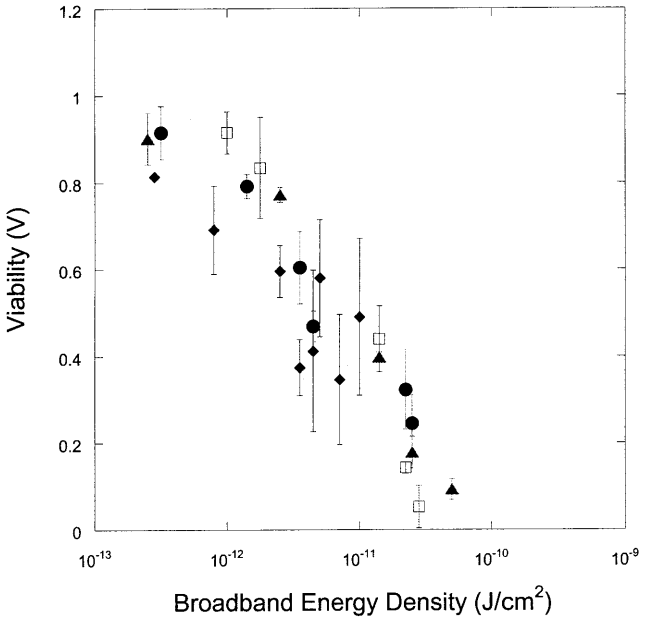

FIGURE 3 Variation of cell viability (V) with broadband energy density at four frequencies (♦, 20 kHz; ▲, 57 kHz; □, 76 kHz; and ●, 93 kHz). Error bars show standard deviation on at least four repetitions. Broadband energy density was calculated using the equation $E_{bb} = P_{bb}^2 t/\rho c$ where P_{bb} is the amplitude of broadband noise (*bar*), ρ is water density (1000 kg/m^3), c is speed of sound in water (1500 m/s), and t is application time.

transient cavitation energy. However, interestingly, the dependence of viability on transient cavitation energy appears to be given by a single function regardless of the frequency. It is important to remember that the absolute value of the broadband energy measured in our experiments is highly likely to depend on the experimental system. Accordingly, interpretation of the absolute value of cavitation energy should not be attempted at this stage. The most important conclusion of the data shown in Fig. 3 is that cell viability is close to unity when no broadband noise is observed and decreases with increasing broadband noise. This result supports the hypothesis that ultrasound-mediated membrane permeabilization is mediated by transient cavitation. This result is consistent with the data of Everbach and co-workers, who reported that hemolysis by 1 MHz ultrasound correlates with transient cavitation (Everbach et al., 1997).

Fig. 4 shows the variation of fraction of cells reversibly permeabilized as a function of transient cavitation energy. Once again, transport of calcein correlates well with broadband noise. Fig. 5 shows the fraction of viable cells that exhibited transport (T/V) as a function of transient cavitation energy density at four frequencies. At each frequency, this fraction increased monotonically and approached unity at high energy densities. This is understandable, inasmuch as at higher energies we expect that the entire cell population is affected by the ultrasound. Accordingly, the entire cell population would be divided into only two categories, the population that is reversibly permeabilized and the population that is irreversibly permeabilized. Since the fraction of cells permeabilized irreversibly is deemed non-

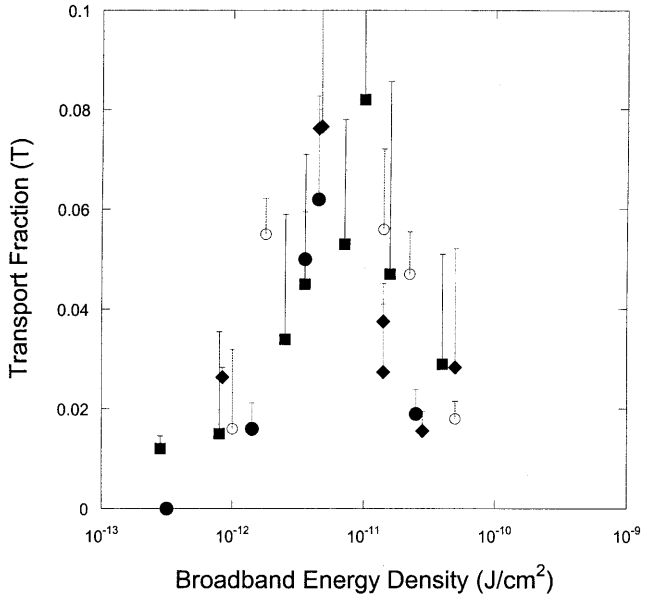

FIGURE 4 Variation of cell population fraction exhibiting calcein transport (T) with broadband energy density, E_{bb}, at four frequencies (◆, 20 kHz; ▲, 57 kHz; □, 76 kHz; and ●, 93 kHz). Error bars show standard deviation on at least four repetitions.

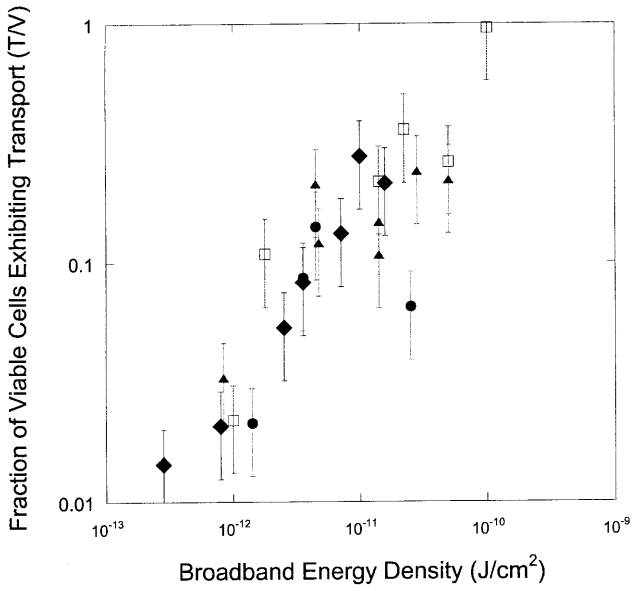

FIGURE 5 Variation of the ratio of cell population fraction exhibiting calcein transport to viable cell fraction (T/V) with broadband energy density, E_{bb}, at four frequencies (◆, 20 kHz; ▲, 57 kHz; □, 76 kHz; and ●, 93 kHz). Error bars show standard deviation on at least four repetitions.

viable, the fraction of viable cells exhibiting calcein transport should approach unity.

Fig. 6, A and B respectively, show the dependence of viability (V) and fraction of cells reversibly permeabilized (T) as a function of subharmonic energy for four frequencies. There appears to be no unique correlation between either viability or transport with subharmonic energy density.

THEORETICAL ANALYSIS OF THE ROLE OF TRANSIENT CAVITATION

Inertial or transient cavitation corresponds to violent collapse of bubbles leading to high local pressures and temperatures (Suslick, 1989). Inertial cavitation has been suggested to play an important role in ultrasound-induced membrane permeabilization (Miller et al., 1996). However, the precise mechanisms through which inertial cavitation affects membrane permeability are not known. Two possible mechanisms, including shock waves produced upon bubble collapse and membrane deformation induced due to radial bubble velocities, are considered in the following analysis.

Membrane disruption due to shock waves

Shock waves with amplitudes in the range of 10–1000 bar have been shown to induce membrane disruption and other biological effects (Delius, 1997; Kodama et al., 2000, 2002; Mayer et al., 1990; Williams et al., 1999). Critical amplitudes for cell and tissue damage due to shock waves have been found to vary based on the experimental system (Kodama

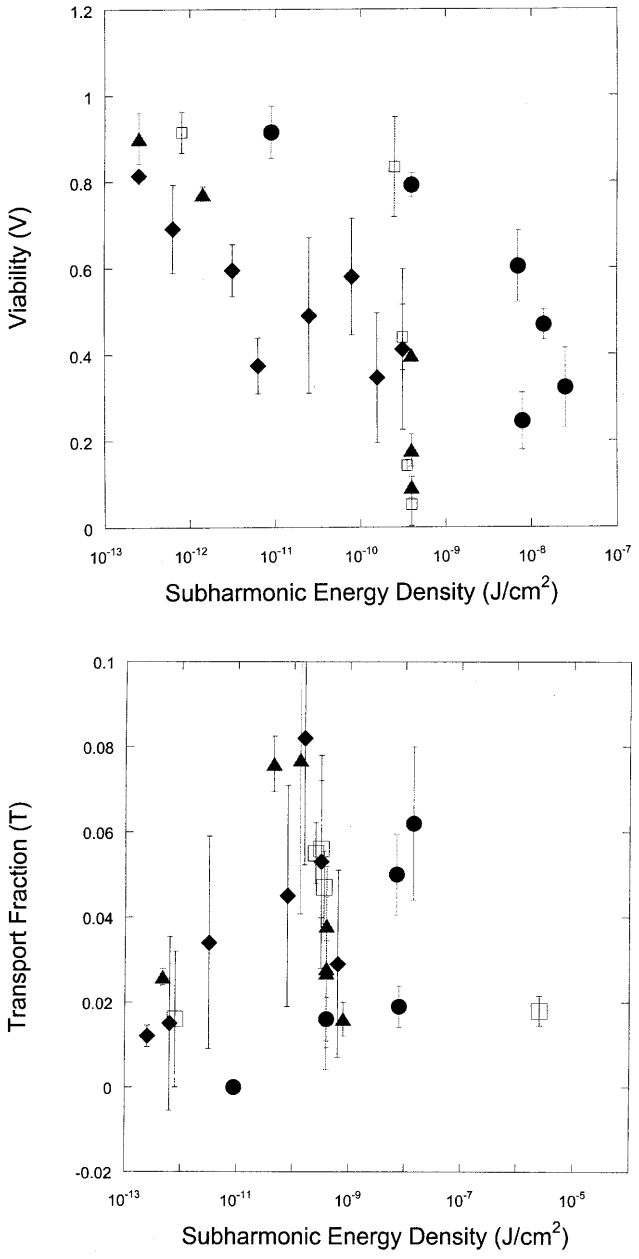

FIGURE 6 (*A*) Variation of the cell viability (V) with subharmonic energy density at four frequencies (♦, 20 kHz; ▲, 57 kHz; □, 76 kHz; and ●, 93 kHz). Error bars show standard deviation on at least four repetitions. Subharmonic energy density was calculated using the equation $E_{sh} = P_{sh}^2 t/\rho c$, where P_{sh} is the amplitude of subharmonic amplitude (*bar*), ρ is water density (1000 kg/m^3), c is speed of sound in water (1500 m/s), and t is application time. (*B*) Variation of the fraction of cells exhibiting calcein transport (T) with subharmonic energy density at four frequencies (♦, 20 kHz; ▲, 57 kHz; □, 76 kHz; and ●, 93 kHz). Error bars show standard deviation on at least four repetitions.

et al., 2002; Raeman et al., 1994; Sonden et al., 2000). Single shock waves of amplitudes of up to 3 kbar have been found sufficient to induce reversible membrane permeabilization but not lethal disruption (Kodama et al., 2000).

It is also known that shock waves with amplitudes approaching or exceeding 1000 bar are generated at the end of bubble collapse in an ultrasound field (Pecha and Gompf, 1999). Pressures inside a collapsing bubble and the subsequent amplitude of the shock wave have been determined through theoretical calculations as well as through experiments. Theoretical estimates assuming adiabatic collapses of bubbles have yielded pressures of >10 kbar inside bubbles at the minimum bubble radius (Vichare et al., 2000). However, experimental measurements of these pressures have proved challenging. This reflects the fact that the high pressures are observed in a narrow space and time domain (Pecha and Gompf, 1999). Nonetheless, direct or indirect experimental measurements of maximum pressures in collapsing bubbles have yielded values in the range 1.7–73 kbar (Matula et al., 1998; Pecha and Gompf, 1999; Wang et al., 1999). Such high pressures are accompanied by shock waves that propagate spherically around the center of bubble collapse. The precise mechanisms by which shock waves affect the cells and tissues are not known, although a number of attempts have been made to gain a better understanding. Lokhandwalla and Sturtevant performed a theoretical analysis of shock wave-induced cell membrane disruption (Lokhandwalla and Sturtevant, 2001). They argued that the spatial and temporal gradients in shock wave amplitude induce membrane deformation and subsequent disruption. Role of stress gradient in shock wave-mediated membrane disruption has also been stated by Doukas et al. (1995). Howard and Sturtevant also argued that shock waves induce membrane strain and the magnitude of the strain is directly proportional to the shock wave amplitude and the duration of the shock wave (Howard and Sturtevant, 1997). On the other hand, Kodama and co-workers argued that shock waves permeabilize membrane by inducing relative displacement between the cell and the surrounding fluid (Kodama et al., 2000).

Cell membranes possess relatively low tolerance to membrane stretching. The critical value of area strain, $\Delta A/A$, where A is the original membrane area, and ΔA is the stress-induced increase in area necessary for membrane disruption, has been reported to be ~0.02–0.03 for red cell membranes (Evans et al., 1976; Netz and Schick, 1996). Critical strain of membranes may vary depending on the loading rate. However, in the absence of this information, a range of 0.01–0.03 was used as a representative range. As will be shown later, these strains are easily exceeded during exposure of cells to cavitation-mediated shock waves. Accordingly, shock wave-induced membrane disruption is highly likely to play an important role in cellular delivery.

Membrane disruption due to bubble wall motion

Shear stresses have also been suggested to play a significant role in ultrasound-mediated membrane permeabilization (Wu, 2002; Wu et al., 2002). Lokhandwalla et al. theorized

that membrane deformation induced by radial bubble motion plays a dominant role in membrane deformation (Lokhandwalla and Sturtevant, 2001). An estimate of membrane deformation induced by bubble motion can be performed following their approach. During the expansion stage of transient cavitation, bubbles grow rapidly from an initial radius, R_o, to a radius, R_{max} in less than half the acoustic cycle and violently collapse thereafter. For example, Wu and Roberts calculated that transient cavities in water exposed to ultrasound at 26.5 kHz grow to a radius of 37 μm in ~16 μs (starting from an initial radius of ~5 μm) and collapse in ~3 μs (Wu and Roberts, 1993). Thus, the average bubble velocities during bubble growth and collapse in this case are respectively 2 m/s and 12 m/s. Membrane deformation induced by these velocities in a cell located at a distance, r, from the center of the bubble has been described by Lokhandwalla as $\Delta A/A \sim (U_b R_b^2/r^3)\tau$, where U_b is the bubble wall velocity, R_b is the bubble radius, and τ is the time of expansion or collapse (Lokhandwalla and Sturtevant, 2001). As will be shown later, the critical area strains of 0.03 can be exceeded during exposure of cells to velocities generated by bubble wall motion. Accordingly, membrane deformation due to bubble wall motion also needs to be considered in describing membrane disruption.

Other mechanisms, including interactions of cells with stable cavities, collisions of bubbles with cells, transducer-induced microstreaming in the absence of bubbles, and chemical effects of cavitation, are not considered in this analysis. Analysis of the importance (or lack thereof) of these mechanisms in membrane permeabilization has been discussed in the literature (Miller et al., 1996). These mechanisms were excluded from this analysis primarily due to the preliminary evidence presented by the acoustic spectroscopy data that transient cavitation is responsible for transport under conditions used in this study.

Permeabilization of cell membranes (either due to shock waves or due to bubble motion) may occur from interaction with a single bubble or a series of bubbles. We first analyze the scenario that membrane permeabilization is induced by a single collapse.

Single bubble interaction model

Let us assume that during application of ultrasound at a given frequency and intensity for a certain time, a total of M transient cavitation events take place. We now introduce two radii, r_1 and r_2 ($r_1 < r_2$). The value of r_1 is chosen such that cells located within a sphere of radius r_1 around the bubble are irreversibly permeabilized due to high shock wave amplitude or high deformations induced by bubble wall motion. The value of r_1 is likely to be different in both cases. The value of r_2 is chosen such that for the cells located outside a sphere of radius r_2 around the bubble are not affected by bubbles. Cells located in a region within the radii r_1 and r_2 are assumed to be reversibly permeabilized.

Consider the first collapse of a transient bubble in a volume, v, of liquid, in which N cells are suspended The number of cells, N_1^v, located within a sphere of radius of r_1 around the bubble is given as follows:

$$N_1^v = \frac{4}{3}\pi(r_1^3 - R_b^3)\left(\frac{N}{v}\right), \tag{1}$$

where R_b is the bubble radius. Hence, the cell viability at the end of the 1st collapse, α_1, is given as follows:

$$\alpha_1 = 1 - \frac{4}{3}\pi(r_1^3 - R_b^3)\left(\frac{1}{v}\right). \tag{2}$$

Similarly, the fraction of cells exhibiting reversible permeabilization at the end of the first cavitation event, β_1, is given by the following equation:

$$\beta_1 = \frac{4}{3}\pi(r_2^3 - r_1^3)\left(\frac{1}{v}\right). \tag{3}$$

Assuming that distribution of bubbles and cells in suspension is random, it can be shown that the cell viability, V_M, and fraction of cells exhibiting reversible permeabilization, T_M, after M cavitation events, are respectively given by the following equations:

$$V_M = 1 - \lambda \sum_{m=1}^{M} (1-\lambda)^{m-1}, \tag{4}$$

and

$$T_M = \mu \sum_{m=1}^{M} (1-\mu)^{m-1} - [1 - V_M], \tag{5}$$

where, $\lambda = (4/3v)\pi(r_1^3 - R_b^3)$ and $\mu = (4/3v)\pi(r_2^3 - R_b^3)$. The assumption that the cells and collapses are random is justifiable, inasmuch as the cell suspension is well mixed. Furthermore, the dimensions of the transducer and the well used to hold the cell suspension are comparable. With further analysis, it can be shown that Eqs. 4 and 5 can be respectively simplified to the following:

$$V_M \approx e^{-\lambda M}; \tag{6}$$

$$T_M \approx e^{-\lambda M} - e^{-\mu M}. \tag{7}$$

Equation 6 can be substituted in Eq. 7 to arrive at the following equation:

$$T_M \approx V_M - e^{-\mu M}. \tag{8}$$

Equations 6 and 8 offer simple equations to relate viability and transport to the number of cavitation events. Equation 6 predicts that cell viability decreases monotonically with the number of cavitation events, while the transport exhibits a maximum with respect to the number of cavitation events. This is apparent by differentiating Eq. 7 as follows:

$$\frac{dT_M}{dM} \approx -\lambda e^{-\lambda M} + \mu e^{-\mu M}. \tag{9}$$

The number of cavitation events, M_{max}, for which T_M is maximum is given by the following:

$$M_{max} = \frac{\ln(\lambda/\mu)}{(\mu - \lambda)}. \quad (10)$$

The parameters, λ and μ, may depend on several parameters including ultrasound frequency. Determination of these parameters is discussed later. Before comparing the model predictions with experimental data, we evaluated the possibility of membrane permeabilization due to multiple cavitation events. This calculation is necessary to confirm that the assumption made in the earlier analysis, that cells are permeabilized by a single cavitation event, is valid.

Consider a suspension of N cells in a liquid volume, v. The probability that a cell is located within a radius r_1 of a collapse is given by the following equation:

$$p = \frac{4}{3}\pi(r_1^3 - R_b^3)\left(\frac{1}{v}\right) = \lambda. \quad (11)$$

Accordingly, after the occurrence of M transient cavitation events the probability, p_1, that a cell experiences at least one event is given by the following equation:

$$p_1 \approx \lambda M. \quad (12)$$

Assuming that the cavitation events occur randomly in the cell suspension and that the cells are well mixed, the probability, p_j, that a cell is located within a radius r_1 of j cavitation events, when a total of M events have taken place during the entire period of ultrasound application, is given by the following equation:

$$p_j \sim \left(\frac{\lambda M}{j}\right)^j. \quad (13)$$

As will be shown later, under a typical ultrasound condition used in this study (for example, 20 kHz and 10 J/cm^2, application time of 10 s) the value of λ is $\sim 10^{-7}$ and M of $\sim 10^6$. With these parameters, values of p_j are $\sim 10^{-1}$, 10^{-3}, and 10^{-5}, respectively for $j = 1$, 2, and 3. Thus, the probability of a cell residing within a radius of r_1 of multiple bubbles simultaneously or sequentially during an application of 10 s is significantly lower than that for a single event. Accordingly, reversible or irreversible permeabilization of cell membranes is hypothesized to occur through interaction with a single bubble.

COMPARISON OF MODEL PREDICTIONS WITH EXPERIMENTAL DATA

To make quantitative predictions based on the model equations, information is required on two parameters, λ and μ, which in turn depend on r_1 and r_2. Furthermore, Eqs. 6 and 7 relate V_M and T_M to the number of cavitation events, M. However, experimental data in Figs. 1 and 2 show the dependence of viability and transport on ultrasound energy density, E. Accordingly, to directly compare the model predictions with experimental data, a relationship between E and M is necessary.

We assume that an approximate relationship between the number of cavitation events and energy density can be written as follows:

$$M = \kappa E A_t, \quad (14)$$

where M is the number of transient cavitation events, E is the energy density (J/cm^2), and A_t is the transducer area (cm^2). κ is a constant (number of bubbles per Joule of acoustic energy). Energy density, E, is related to intensity, I, and application time, t as $E = It$. Since no system-specific information (for example, liquid volume, nuclei concentration, etc.) in included in Eq. 14, the parameter κ is system-specific and not a universal constant. Eq. 14 simply states that the number of cavitation events per unit time is proportional to ultrasound intensity. The validity of Eq. 14 can be justified by previous reports of Mitragotri and co-workers who showed that the number of pits on aluminum foil per unit time at a constant frequency increases proportionally to ultrasound intensity (higher than cavitation threshold; Mitragotri et al., 2000a). Our direct measurements of the number of cavitation events using hydrophone measurements also support a direct relationship between the number of cavitation events and ultrasound intensity when the intensity is well beyond the cavitation threshold (unpublished data). By using Eq. 14, Eqs. 4 and 5 can be modified to the following:

$$V \approx e^{-\lambda\kappa A_t E}; \quad (15)$$

$$T \approx V - e^{-\mu\kappa A_t E}. \quad (16)$$

T_M and V_M in Eqs. 4 and 5 have been changed to T and V respectively, to reflect the fact that these parameters are now a function of energy and not M. Fig. 7, *A–D* show fits of Eqs. 15 and 16 to experimental data. Both equations correctly predict the trends shown in experimental data (Fig. 7, *A–D*). Specifically, cell viability decreases exponentially with energy density while transport exhibits a maximum with respect to energy density. By fitting Eqs. 15 and 16 to experimental data in Fig. 7, *A–D*, values for $\lambda\kappa$ and $\mu\kappa$ were obtained. The values of $\lambda\kappa$ at 20 kHz, 57 kHz, 76 kHz, and 93 kHz were respectively 0.065, 0.03, 0.031, and 0.012. The values of $\mu\kappa$ at 20 kHz, 57 kHz, 76 kHz, and 93 kHz were respectively 0.088, 0.036, 0.038, and 0.014. Equations 15 and 16 fit well to the experimental data ($r^2 >$ 0.9 for Eq. 15 and $r^2 > 0.7$ for Eq. 16). Estimated errors in fitted parameters were <20%. Plots of V against $\lambda\kappa A_t E$ and $V + T$ against $\mu\kappa A_t E$ showed that data for all four frequencies can be defined by the same trend, that is, Eqs. 15 and 16 respectively (data not plotted).

To further understand the relevance of λ, μ, and κ in membrane permeabilization, individual determination of these parameters is necessary. Note that the model described

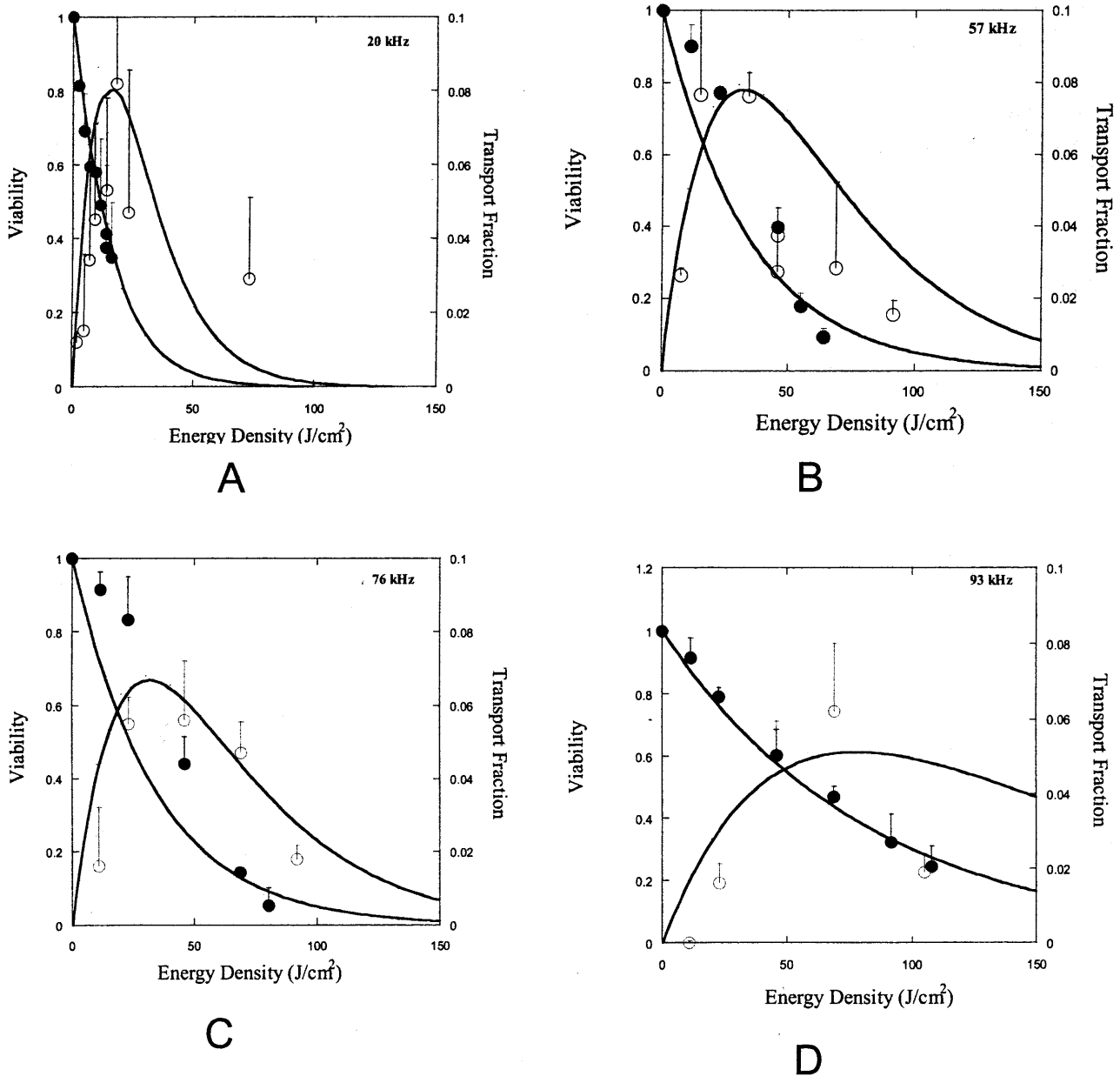

FIGURE 7 (*A–D*) Experimental data on viability of 3T3 cells at four frequencies and various energy densities between 0 and 150 J/cm^2 (*A*: 93 kHz, *B*: 76 kHz, *C*: 57 kHz, and *D*: 20 kHz). ○ corresponds to transport fraction and ● corresponds to viability. Error bars correspond to standard deviation (based on at least four repetitions). Lines correspond to fits of Eq. 13 for viability data and Eq. 14 for transport data. Eqs. 13 and 14 fitted to viability and transport data with average r^2 values of 0.9 and 0.1, respectively. The estimated errors in fitted parameters ($\lambda\kappa$ and $\mu\kappa$) were lower than 20%.

so far allows determination of $\lambda\kappa$ and $\mu\kappa$ but not λ, μ, and κ individually. Once one of the three parameters (λ, μ, or κ) is independently determined, the others can be calculated. We chose to determine λ through independent calculations.

Lambda is related to the radius of the sphere within which cell membranes are irreversibly disrupted during a single collapse, $\lambda = (4/3v)\pi(r_1^3 - R_b^3)$. The radius r_1 depends on the mechanism by which bubbles disrupt the membranes. As discussed earlier, two mechanisms of membrane disruption are considered. The first mechanism includes disruption mediated by the shock wave originating at the end of bubble collapse and the second mechanism includes disruption mediated by radial bubble motion during expansion and collapse of transient cavities. If r_1 can be independently determined, individual values of λ, μ, and κ can be determined. Estimation of r_1 for shock wave-mediated membrane disruption is discussed in Appendix 2. Estimation of r_1 for bubble-motion mediated membrane disruption is discussed in Appendix 3. Estimation of r_1 in both cases requires a knowledge of important cavitation parameters including minimum and maximum bubble radii (R_{min} and R_{max}), and collapse pressure, P_o. Determination of these parameters is

discussed in Appendix 1. Cavitation parameters determined through analysis in Appendix 1 are summarized in Table 1.

Table 2 shows values of λ, μ, and κ for shock wave-mediated membrane permeabilization for three representative values of ε_c, 0.03, 0.02, and 0.01. These values illustrate several interesting features. The values of λ and μ are close to each other (at the same value of ε_c), which is consistent with the hypothesis that the mechanisms responsible for reversible and irreversible membrane permeabilization are similar, and the difference in the pressure necessary to induce reversible and irreversible membrane disruption is small. It is important to note that the value of μ (and hence r_2) is determined based on the transport as determined by an intracellular calcein concentration of at least 5 μM. Since this choice of critical intracellular concentration is somewhat arbitrary, the value μ is subject to change based on the choice of the threshold. By using various threshold concentrations in the range of 0–50 μM, a set of μ values can be determined. As the threshold concentration increases from 0 to 50 μM, the value of μ decreases from infinity to λ. Determination of the functional relationship between μ and threshold concentration is beyond the scope of this study.

The model predicts that the rate of transient cavitation events in cell suspensions is in the range of mid 10^3 to high 10^4 collapses per second per Joule of acoustic energy at 20 kHz depending on the choice of value of critical strain. Although the range of κ reported in Table 2 appears very high, it should be realized that uncertainties in the estimation of cavitation parameters are usually high owing to the extreme sensitivity to parameters. This is also true for experimental characterization of cavitation events, where small changes in system parameters yield substantial variability in experimental results. Using a representative number of κ as 5×10^4, the ratio of *cells:number of collapses per second* is ~20:1 (total number of cells in suspension of $\sim 10^6$ and $\kappa \sim 5 \times 10^4$ collapses per second). It is difficult to independently confirm whether the number of collapses determined by the model is accurate. However, an analysis based on the energies of bubble expansion and collapse (see Appendix 4) yields numbers that appear reasonable. Kappa decreases with increasing frequency. At 93 kHz, κ values are predicted to be in the range of low 10^2 to low 10^3, depending on the value of critical strain.

Table 3 shows λ, μ, and κ, assuming that bubble wall motion is responsible for membrane disruption. Once again, κ decreases with increasing frequency. The predicted number of collapse events is generally higher than that in the case of shock wave-mediated membrane disruption. The model predicts that the number of cavitation events per unit energy density is about low 10^4 to low 10^5/s at 20 kHz. In this mode of membrane disruption, the effectiveness of a cavitation bubble in inducing reversible or irreversible membrane permeabilization decreases inversely with the cube of the distance between the cell and bubble (Appendix 3). Interestingly, such a dependence of membrane permeabilization on distance has been reported by Ward et al. (2000) based on experimental observations.

TABLE 1 Model parameters related to cavitation bubble collapse

Frequency (kHz)	P_a bar	R_{max} μm	P_i bar	R_{min} μm	P_o kbar
20	1.2	30	0.03	1.0	48
57	1.8	38	0.03	1.3	48
76	2.3	42	0.03	1.4	48
93	2.7	45	0.03	1.5	48

Calculations of these parameters are described in Appendix 1.

The values r_1 and r_2 respectively depict the ''destructive zone'' and ''working zone'' around a transient cavitation bubble. For ε values of 0.02, the values of r_1 and r_2 are $O(100\ \mu m)$. Values of r_1 and r_2 are close to each other, suggesting a narrow window of space within which the cells are reversibly permeabilized. Furthermore, the values of r_1 and r_2 are smaller than the average distance between the bubble collapse and cell, which may explain the heterogeneity in transport, at least in part.

Based on the agreement of the theory with experimental data, it is difficult to ascertain whether shock waves or radial bubble velocities are entirely responsible for membrane permeabilization by themselves. The effective distances around the bubble and number of collapses are comparable in both cases. Since the effects of bubble expansion, collapse, and shock wave on cell membranes are occurring at different stages of collapse, their effects can be additive and collectively responsible for membrane permeabilization. The stresses acting during shock waves are exceedingly high although their effective time is very short (nanoseconds). On the other hand, the stresses encountered during bubble motion in the expansion and collapse are comparatively low, but the times over which these stresses act are relatively long (microsecond). The membrane strain induced during both stages is predicted to be of the same order of magnitude. This is also clear from Eqs. A6 and A8, which show that the maximum strain induced in each case (that is, at $r = R_{min}$ for shock waves and $r = R_b$ for bubble motion), is $\Delta A/A \sim 1$. Based on the values of parameters reported in Tables 2 and 3, the contribution of shock wave-mediated permeabilization is likely to be higher than bubble-mediated permeabilization for smaller values of ε_c. This originates from the fact that the strain induced by shock waves decreases as $1/r$, whereas the strain induced by bubble wall decreases as $1/r^3$. To resolve the role of shock waves versus bubble wall motion within one-order-magnitude, a more accurate determination of model parameters R_{max}, R_{min}, and ε_c is necessary.

The model presented here provides two outcomes. First, it correlates cell viability and transport to fundamental parameters including number of collapses, collapse pressure, and bubble wall velocities. Second, it provides an analysis of the importance of various stages of cavitation in membrane permeabilization. The model parameters are physical and can

TABLE 2 Model parameters for shock wave-mediated membrane disruption assuming three critical values of ΔA/A (or ε_c) for membrane disruption

	$\lambda \times 10^7$			$\mu \times 10^7$			$\kappa \times 10^{-3}$			r_1 (μm)			r_2 (μm)		
Frequency (kHz)	I	II	III	I	II	III	I	II	III	I	II	III	I	II	III
20	8	25	203	10	32	259	88	26	3.3	71	107	213	77	116	231
57	15	51	407	19	64	508	20	6	0.7	90	134	269	96	145	289
76	17	57	447	20	67	538	18	5	0.6	92	139	277	98	148	295
93	20	69	558	24	80	641	6	2	0.2	99	149	299	104	157	313

$I = 0.03$; $II = 0.02$; and $III = 0.01$. Calculations of model parameters are described in Appendix 2.

be directly related to bubble dynamics. The model parameters also allow quantification of the ''destruction'' zone and ''working'' zone around a cavitation bubble.

CONCLUSIONS

Effect of low-frequency ultrasound on viability and calcein transport of 3T3 cells was investigated. Viability decreased monotonously with increasing energy density at each frequency. At a given energy density, viability increased with increasing frequency. At each frequency, transport efficiency exhibited a maximum with respect to energy density. The energy density corresponding to maximum transport increased with increasing frequency. Viability as well as transport efficiency correlated with the energy density of broadband noise energy regardless of the frequency. These results support the role of transient cavitation in ultrasound-mediated membrane permeabilization. A mathematical model was developed to relate the effect of ultrasound with the number of transient cavitation events. The model also allowed assessment of the role of various stages of transient cavitation, including bubble expansion, collapse, and subsequent shock wave formation, in reversible as well as irreversible membrane permeabilization. Bubble expansion and collapse, as well as shock wave, were found to contribute toward membrane permeabilization.

APPENDIX 1

Mechanics of bubble collapse and determination of related parameters

During its growth, the bubble radius increases isothermally and reaches a value of R_{max} before collapsing adiabatically. Assuming that the pressure inside the bubble just before adiabatic collapse is P_i, the pressure inside the bubble (including gas and vapor pressure) at the end of the collapse, P_o (assumed equal to the amplitude of the emitted shock wave), is given by the following equation:

$$P_o = P_i \left(\frac{R_{max}}{R_{min}}\right)^{3\gamma}, \tag{A1}$$

where R_{max} is the bubble radius just before the initiation of collapse and R_{min} is the bubble radius at the end of the collapse (that is the radius just before the initiation of bubble rebound). Gamma is the ratio of specific heats. Both R_{max} and R_{min} may vary with ultrasound frequency and intensity. Measurements of R_{max} have been challenging, inasmuch as the bubbles exist at this radius only transiently. Among the few measurements of R_{max} that have been reported in the literature include those of Ashokkumar and coworkers, who reported a R_{max} value of 56 μm at 23 kHz at a driving pressure of 1.3 bar (Ashokkumar et al., 2002), and those of Didenko and Suslick, who reported a value of 28.9 μm reported for 52 kHz and a pressure amplitude of 1.5 bar (Didenko and Suslick, 2002).

R_{max} has been related to the frequency and pressure amplitude by the following approximate equation (Colussi et al., 1998; Mason and Lorimer, 1988):

$$R_{max} = \frac{3000}{f}\left[\frac{(P_a - 1)}{\sqrt{P_a}}\left(1 + \frac{2(P_a - 1)}{3}\right)^{1/3}\right], \tag{A2}$$

where, R_{max} is in μm and f is in kHz. P_a is the acoustic pressure amplitude in bar. Although R_{max} may be calculated for each frequency and pressure amplitude, we used average pressure amplitudes for calculations. This was feasible inasmuch as the pressure amplitudes used in this study were in a relatively narrow range. The average pressure amplitudes, P_a, used in this study at 20 kHz, 57 kHz, 76 kHz, and 93 kHz, are respectively 1.2 (+/− 0.35) bar, 1.8 (+/− 0.28) bar, 2.3 (+/− 0.6) bar, and 2.7 (+/− 0.6) bar. Using these pressure amplitudes and Eq. A2, calculated values of R_{max} for 20 kHz, 57 kHz, 76 kHz, and 93 kHz are respectively 30 μm, 38 μm, 42 μm, and 41 μm. These numbers are consistent with available literature data. Specifically, an R_{max} value of 30 μm at 20 kHz and a pressure amplitude of 1.2 bar is consistent with that reported by a number of investigators (Hilgenfeldt and Lohse, 1999; Matula, 1999; Storey and Szeri, 2000).

TABLE 3 Model parameters for membrane disruption by bubble expansion or early moments of collapse assuming three critical values of ΔA/A (or ε_c) for membrane disruption

	$\lambda \times 10^7$			$\mu \times 10^7$			$\kappa \times 10^{-3}$			r_1 (μm)			r_2 (μm)		
Frequency (kHz)	I	II	III	I	II	III	I	II	III	I	II	III	I	II	III
20	4	7	14	5	8	17	161	102	49	60	69	88	66	75	95
57	8	13	27	10	17	35	35	22	11	77	89	111	83	95	120
76	11	18	37	14	21	45	26	17	8	85	97	123	91	103	130
93	14	21	46	16	25	53	9	5	3	91	104	132	96	109	138

$I = 0.03$; $II = 0.02$; and $III = 0.01$. Calculations of model parameters are described in Appendix 3.

Calculations based on Eq. A2 are also consistent with an R_{max} value of 28.9 μm reported for 52 kHz and a pressure amplitude of 1.5 bar (Didenko and Suslick, 2002), a value of 8.3 μm reported for 300 kHz and a pressure amplitude of 2 bar (Colussi et al., 1998), as well as other experimental measurements (Ohl et al., 1999).

The pressures inside the bubble just before beginning of the collapse, P_i, are substantially smaller than the surrounding pressure due to expansion. Assuming the bubble expansion to be isothermal, the pressure in the bubble just before the beginning of the collapse is given by the following equation (Prosperetti and Hao, 1999):

$$P_i = \left(P_{inf} + \frac{2\sigma}{R_o}\right)\frac{R_o^3}{R_{max}^3}, \tag{A3}$$

where P_{inf} is the surrounding pressure (1 bar), σ is the surface tension, and R_o is the initial bubble radius before the expansion phase. Utilization of Eq. A3 is limited by the lack of experimental data on R_o. Furthermore, Eq. A3 assumes that the mass of the bubble remains the same during the expansion. However, water vapor enters the bubble during expansion and at the maximum bubble radius, the bubble may contain nearly 90% water vapor (Storey and Szeri, 2000). Accordingly, the pressure inside the bubble just before collapse can be assumed to be equal to the vapor pressure of water at 25°C (0.03 bar (Perry and Green, 1973). Calculations of Brenner and co-workers for cavitation bubbles at 26.5 kHz and 1.2 bar are in excellent agreement with this assumption (Brenner et al., 2002).

Values of R_{min} may be theoretically estimated by solving Rayleigh-Plesset equation. Vichare and co-workers estimated the minimum bubble radius, assuming that the limiting radius is reached when bubble wall velocity reaches the speed of sound in water (~1500 m/s; Vichare et al., 2000). Numerical simulations have yielded a R_{min} value of ~1 μm for 20 kHz and a pressure amplitude of 1.2 bar (Brenner et al., 2002). Hilgenfeldt and Lohse (1999) reported numerical calculations on the dependence of R_{min} on ultrasound frequency. Using their data, predicted values of R_{min} for 20 kHz, 57 kHz, 76 kHz, and 93 kHz are respectively 1 μm, 1.4 μm, 1.6 μm, and 1.8 μm. These values of R_{min} have been determined at a constant pressure amplitude of 1.2 bar. Although use of these R_{min} values are strictly applicable to a pressure amplitude of 1.2 bar, approximate values of P_o can be determined using these values of R_{min}. Collapse pressures determined using Eq. A1 are 48 kbar, 31 kbar, 27 kbar, and 22 kbar at 20 kHz, 57 kHz, 76 kHz, and 93 kHz, respectively. These pressures have been calculated assuming that the vapor does not condense in the bubble during collapse. The pressures would be lower if the vapor does condense. The collapse pressures determined by Eq. A1 compare well with the available experimental data for frequencies ~20 kHz. Specifically, at a frequency of 20 kHz, Pecha and Gompf experimentally determined the collapse pressure of ~40–60 kbar (Pecha and Gompf, 1999). Other indirect measurements of collapse pressures have yielded values in the range of 1.7–73 kbar (Holzfuss et al., 1998; Matula et al., 1998; Wang et al., 1999; Weninger et al., 1997). The error in P_o at other frequencies is difficult to estimate inasmuch as the errors in R_{min} are difficult to estimate. Furthermore, experimental reports of collapse pressures at these frequencies were not found in the literature. Due to the uncertainty in determining collapse pressures at frequencies other than 20 kHz, we considered an alternative approach. We assumed that the minimum bubble radius for a given value of R_{max} is determined primarily by gas compressibility; that is, the ratio R_{max}/R_{min} is nearly independent of frequency and acoustic pressure amplitude for a given value of R_{max}. This assumption is likely to be valid when the collapse time is much smaller than the acoustic period. As shown in Appendix 2, the collapse time of a bubble possessing an R_{max} value of 40 μm at an acoustic pressure amplitude, P_a, of 1 bar, is ~2.6 μs. This time is much smaller than the acoustic time periods (50 μs, 17 μs, 13 μs, and 10 μs at 20 kHz, 57 kHz, 76 kHz, and 93 kHz, respectively). This assumption is also valid in this study since the values of R_{max} are close to each other (see Table 1).

Since the confidence in the estimated value of collapse pressure at 20 kHz is higher than that at other pressures (due to independent confirmation of R_{max}, R_{min}, and P_o with literature data under conditions identical to those used in this study), we assume that the estimated collapse pressure at 20 kHz is more accurate. Using 48 kbar as a reference value, the corresponding value of R_{max}/R_{min} is 30. Accordingly, R_{min} values at 57 kHz, 76 kHz, and 93 kHz under pressure amplitudes shown in Table 1 are 1.3 μm, 1.4 μm, and 1.5 μm, respectively. These values are listed in Table 1 and are used in further calculations. The P_o and R_{min} values determined in both methods are comparable (P_o = 48 kbar versus 22–48 kbar, and R_{min} = 1–1.5 μm versus 1–1.8 μm).

APPENDIX 2

Determination of r_1 for shock wave-mediated membrane disruption

Several reports of shock wave-mediated cell lysis can be found in the literature (Delius, 1997; Kodama et al., 2000, 2002; Sonden et al., 2000; Williams et al., 1999; Zhong et al., 1999, 1998). The amplitudes of shock waves used in these studies range from 100 to 1000 bar and the pulse duration was typically on the order of microseconds.

Membrane damage upon exposure to shock waves may occur through shock-induced relative particle displacement, compressive failure, tensile loading, or shear strains. While all these mechanisms may potentially responsible for membrane disruption, the first mechanism provides the simplest explanation for it. The damage potential of the shock wave depends on the spatial gradient of pressure and duration of the pulse (Lokhandwalla and Sturtevant, 2001). It can be shown that the strain, ε, in a section of the material of thickness, Δr, exposed to a shock wave is given by the following equation (unpublished data; this equation can also be derived from the analysis presented by Lokhandwalla and Sturtevant, 2001):

$$\varepsilon \sim \left(\frac{\Delta P}{\Delta r}\right)\frac{\Delta\tau}{\rho c}, \tag{A4}$$

where $\Delta\tau$ is the duration of the shock wave, $\Delta P/\Delta r$ is the spatial gradient of the shock wave amplitude, ρ is the liquid density, and c is the velocity of sound. By choosing Δr such that it approximately corresponds to spatial width of the shock wave, $\Delta\tau$ can be related to $\Delta\gamma$ by $\Delta\tau = \Delta r/c$ and Eq. A4 can be rewritten as follows:

$$\varepsilon \sim \frac{P}{\rho c^2}. \tag{A5}$$

The amplitude of the shock wave decreases rapidly during its radial propagation. The amplitude of the shock wave decreases as $1/r$ during spherical propagation (Matula et al., 1998) Accordingly, Eq. A5 can be modified as follows:

$$\varepsilon \approx \frac{P_o R_{min}}{r\rho c^2}, \tag{A6}$$

where P_o is the shock wave amplitude at its origin, that is, $r = R_{min}$. By equating $\Delta A/A$ to ε and defining r_1 as r at which $\Delta A/A = \varepsilon_c$ (critical strain necessary to irreversibly disrupt the membrane), r_1 can be calculated as follows:

$$r_1 \approx \frac{P_o R_{min}}{\varepsilon_c \rho c^2}. \tag{A7}$$

Values of P_o and R_{min} are listed in Table 1. The r_1 values calculated using Eq. A7 for three values of ε_c are listed in Table 2. The remaining parameters of the model—that is, μ and κ—can now be determined.

APPENDIX 3

Determination of r_1 for membrane disruption mediated by bubble wall motion

Lokhandwalla and co-workers performed an analysis of membrane deformation due to bubble wall motion (Lokhandwalla, et al., 2001). Membrane deformation was related to the bubble radius, R_b, and radial velocity, U_b, by the following equation,

$$\frac{\Delta A}{A} \sim \frac{U_b R_b^2}{r^3}\tau, \tag{A8}$$

where r is the distance of the bubble from the cell and τ is the time for which cells are exposed to bubble motion. Using a critical strain for membrane disruption of ε_c (Evans et al., 1976), Eq. A8 can be rewritten to describe r_1 as

$$r_1^3 \sim \frac{U_b R_b^2}{\varepsilon_c}\tau. \tag{A9}$$

Since bubble motion during expansion and collapse periods is very different, r_1 values for two cases are separately determined. Furthermore, since the bubble radius as well as bubble wall velocity are continuously changing throughout the lifetime of the cavity, values of r_1 are determined using average values of bubble radius and wall velocity. During the expansion period, the bubble grows from an initial radius R_o to R_{max} in approximately one half acoustic cycle or faster. Accordingly, average bubble velocity may be described by the following equation,

$$U_b^{av} \sim \frac{R_{max}}{\tau_a/2}, \tag{A10}$$

where τ_a is the acoustic time period. The average bubble radius, R_b, during this expansion phase and the time of expansion, is given by Eqs. A11 and A12, respectively:

$$R_b^{av} \sim \frac{R_{max}}{2}, \tag{A11}$$

$$\tau \sim \frac{\tau_a}{2}. \tag{A12}$$

While deriving Eqs. A11 and A12, it is implicitly assumed that $R_{max} \gg R_o$. Using Eqs. A10–A12, Eq. A9 can be rewritten as follows:

$$r_1^3 \sim \frac{R_{max}^3}{4\varepsilon_c}. \tag{A13}$$

Using Eq. A13, λ-values associated with bubble expansion were calculated and are shown in Table 3. The range corresponds to the limiting values estimated using $\varepsilon_c = 0.01$ and 0.03.

A similar analysis can be performed for bubble collapse. Since the bubble velocities during the final stage of the collapse are drastically different than those during the most of the collapse, separate analysis is performed during both cases. The collapse time for a bubble is related to R_{max} by the following equation (Mason and Lorimer, 1988):

$$\tau_c \sim 0.915 R_{max}\left(\frac{\rho}{P_s}\right)^{1/2}, \tag{A14}$$

where ρ is the liquid density (1000 kg/m^3) and P_s is the surrounding pressure ($P_s = P_a + 1$ bar). Using $U_b \sim R_{max}/\tau$ and $R_b \sim (R_{max} + R_{min})/2$, average value of λ was calculated (note that inasmuch as $R_{max} \gg R_{min}$, the latter has been neglected). With these assumptions, r_1 is given by the following equation:

$$r_1^3 \sim R_{max}^3/4\varepsilon_c. \tag{A15}$$

The r_1- and λ-values for this condition are comparable to those determined for bubble expansion, and are not separately shown.

During the final stage of collapse, where $R_b \sim R_{min}$, the bubble wall velocity approaches 1500 m/s. A bubble may exist in this stage for ~50 ns (Brenner et al., 2002). With this information, values of r_1 and λ were calculated using Eq. A9. These calculations yielded r_1 values of typically 15 μm. Although these values are significant, they are much smaller than the r_1-values associated with shock waves and bubble motion before final stages. Accordingly, these are not discussed in detail.

APPENDIX 4

Analysis of the energies associated with bubble expansion and collapse can be performed to justify the κ-values determined by the model. The energy necessary for isothermal expansion of a cavity from a radius, R_o, to a radius of R_{max} and the energy available upon adiabetic collapse of the cavity are given by Eqs. A16 and A17, respectively (Vichare et al., 2000):

$$W_{iso} = \frac{4}{3}\pi R_{max}^3 P_i \ln\left(\frac{R_{max}}{R_o}\right)^3, \tag{A16}$$

$$W_{adi} \sim \frac{4}{3}\pi \frac{P_i R_{max}^3}{(\gamma - 1)}\left[1 - \left(\frac{R_{max}}{R_{min}}\right)^{3(\gamma-1)}\right], \tag{A17}$$

where R_o is the initial bubble radius, and P_i is the bubble pressure before collapse. At an intensity of 0.5 W/cm^2 and a frequency of 20 kHz (where, the pressure amplitude is 1.2 bar and R_{max} is 30 μm, assuming $R_o \sim 2$ μm), W_{iso} is ~3 nJ/bubble and W_{adi} is ~29 nJ/bubble. Noting that W_{iso} is the work done by the cavity on the surrounding W_{adi} is the work done on the cavity by the surrounding, the net work done on the cavity is ~26 nJ. This value, in combination with a κ of 1×10^5 per J, predicts that ~0.3% of the acoustic energy is converted into creating transient cavitation energy. Even lower conversion efficiencies are predicted for κ of 5×10^3.

APPENDIX 5

List of model parameters

A	Unstretched area of cell membranes (cm^2)
α_1	Fraction of cells irreversibly permeabilized during the first cavitation event
β_1	Fraction of cells reversibly permeabilized during the first cavitation event
c	Velocity of sound (m/s); 1500 m/s, unless otherwise mentioned
ΔA	Increase in cell membrane area (cm^2)
κ	Number of cavitation events per unit energy dose (J^{-1})
λ	Volume fraction around a bubble within which cells are irreversibly permeabilized
μ	Volume fraction around a bubble within which cells are reversibly permeabilized
N_1^v	Number of cells irreversibly permeabilized during the first cavitation event
P	Probability that a cell is located in a sphere of radius r_1 around a bubble
p_1	Probability that a cell is located within a sphere r_1 of at least one cavitation event
P_a	Acoustic pressure amplitude (bar or Pa)
P_i	Bubble pressure before collapse, (bar or Pa)
p_j	Probability that a cell is located within a sphere r_1 of j cavitation events
P_s	Total pressure around the bubble just before collapse initiation (bar or Pa)
P_{inf}	Pressure far away from the bubble (bar or Pa)

ρ	Liquid density (kg/m^3); 1000 kg/m^3, unless otherwise mentioned
r_1	Radius of sphere around the bubble such that the cells located in this sphere are irreversibly permeabilized (μm)
r_2	Radius of sphere around the bubble such that the cells located between spheres of radii r_1 and r_2 are reversibly permeabilized (μm)
σ	bubble-liquid surface tension (N/m)
T	Fraction of cells reversibly permeabilized after exposure to an energy dose, E
τ or $\Delta\tau$	Time for which a cell experiences shock wave or shear stress (seconds)
t	Ultrasound application time (seconds)
τ_a	Acoustic time period (second)
τ_c	Bubble collapse time (second)
T_M	Fraction of cells reversibly permeabilized after M cavitation events
U_b	Radial velocity of bubble wall (m/s)
V	Cell viability after exposure to an energy dose E
V_M	Cell viability after M cavitation events
W_{adi}	Work of adiabatic bubble collapse
W_{iso}	Work of isothermal bubble expansion

This work was supported by a grant from the Whitaker Foundation.

REFERENCES

Ashokkumar, M., J. Guan, R. Tronsen, T. Matula, J. W. Nuske, and F. Grieser. 2002. Effect of surfactants, polymers, and alcohols on single bubble dynamics and sonoluminescence. *Phys. Rev. E*. 65:046310.

Bao, S., B. Thrall, and D. Miller. 1997. Transfection of a reporter plasmid into cultured cells by sonoporation in vitro. *Ultrasound Med. Biol*. 23:953–959.

Brenner, M. P., S. Hilgenfeldt, and D. Lohse. 2002. Single-bubble sonoluminescence. *Biophys. J*. 74:425–484.

Brown, M. D., A. G. Schatzlein, and I. F. Uchegbu. 2001. Gene delivery with synthetic (nonviral) carriers. *Int. J. Pharm*. 229:1–21.

Canatella, P. J., and M. R. Prausnitz. 2001. Prediction and optimization of gene transfection and drug delivery by electroporation. *Gene Ther*. 8:1464–1469.

Colussi, A. J., L. K. Weavers, and M. R. Hoffmann. 1998. Chemical bubble dynamics and quantitative sonochemistry. *J. Phys. Chem*. 102:6927–6934.

Delius, M. 1997. Minimal static excess pressure minimises the effect of extracorporeal shock waves on cells and reduces it on gall stones. *Ultrasound Med. Biol*. 23:611–617.

Didenko, Y. T., and K. S. Suslick. 2002. the energy efficiency of formation of photons, radicals, and ions during single-bubble cavitation. *Nature*. 418:394–397.

Doukas, A. G., D. J. McAuliffe, S. Lee, V. Venugopalan, and T. J. Flotte. 1995. Physical factors involved in stress-wave-induced cell injury: role of stress gradient. *Ultrasound Med. Biol*. 21:961–967.

Evans, E. A., R. Waugh, and L. Melnik. 1976. Elastic area compressibility modulus of red cell membrane. *Biophys. J*. 16:585–595.

Everbach, E. C., I. R. Makin, M. Azadniv, and R. S. Meltzer. 1997. Correlation of ultrasound-induced hemolysis with cavitation detector output in vitro. *Ultrasound Med. Biol*. 23:619–624.

Fecheimer, M., J. F. Hoylan, S. Parker, J. E. Sisken, F. Patel, and S. Zimmer. 1987. Transfection of mammalian cells with plasmid DNA by scrape loading and sonication loading. *Proc. Natl. Acad. Sci. USA*. 84:8463–8467.

Fischer, P. M., E. Krausz, and D. P. Lane. 2001. Cellular delivery of impermeable effector molecules in the form of conjugates with peptides capable of mediating membrane translocation. *Bioconjug. Chem*. 12:825–841.

Guzman, H. R., D. X. Nguyen, S. Khan, and M. R. Prausnitz. 2001a. Ultrasound-mediated disruption of cell membranes. I. Quantification of molecular uptake and viability. *J. Acoust. Soc. Am*. 110:588–596.

Guzman, H. R., D. X. Nguyen, S. Khan, and M. R. Prausnitz. 2001b. Ultrasound-mediated disruption of cell membranes. II. Heterogenous effects on cells. *J. Acoust. Soc. Am*. 110:597–606.

Hilgenfeldt, S., and D. Lohse. 1999. Predictions for upscaling sonoluminescence. *Phys. Rev. Lett*. 82:1036–1039.

Holzfuss, J., M. Ruggerberg, and A. Billo. 1998. Shock wave emissions of a sonoluliminescing bubble. *Phys. Rev. Lett*. 81:5434–5437.

Howard, D., and B. Sturtevant. 1997. In vitro study of the mechanical effects of shock-wave lithotripsy. *Ultrasound Med. Biol*. 23:1107–1122.

Johnson-Saliba, M., and D. A. Jans. 2001. Gene therapy: optimising DNA delivery to the nucleus. *Curr. Drug Targets*. 2:371–399.

Kim, H. J., J. F. Greenleaf, R. Kinnick, J. Bronk, and M. Bolander. 1996. Ultrasound-mediated transfection of mammalian cells. *Hum. Gene Ther*. 7:1339–1346.

Koch, S., P. Pohl, U. Cobet, and N. G. Rainov. 2000. Ultrasound enhancement of liposome-mediated cell transfection is caused by cavitational effects. *Ultrasound Med. Biol*. 26:897–903.

Kodama, T., A. G. Doukas, and M. R. Hamblin. 2002. Shock wave-mediated molecular delivery into cells. *Biochem. Biophys. Acta*. 1542:186–194.

Kodama, T., M. R. Hamblin, and A. G. Doukas. 2000. Cytoplasmic delivery with shock waves: importance of impulse. *Biophys. J*. 79:1821–1832.

Kodama, T., and K. Takayama. 1998. Dynamic behavior of bubbles during extracorporeal shock-wave lithotripsy. *Ultrasound Med. Biol*. 24:723–738.

Kremkau, F. W. 1998. Diagnostic Ultrasound: Principles and Instruments. W. B. Sanders, editor. Philadelphia.

Leighton, T. 1997. The Acoustic Bubble. Academic Press, San Diego.

Liu J., T. Lewis, and M. Prausnitz. 1998. Non-invasive assessment and control of ultrasound-mediated membrane permeabilization. *Pharm. Res*. 15(6).

Lokhandwalla, M., J. A. McAteer, J. C. Williams, and B. Sturtevant. 2001. Mechanical hemolysis in shock wave lithotripsy (SWL). II. In vitro cell lysis due to shear. *Phys. Med. Biol*. 46:1245–1264.

Lokhandwalla, M., and B. Sturtevant. 2001. Mechanical haemolysis in shock wave lithotripsy (SWL). *Phys. Med. Biol*. 46:413–437.

Mason, T. J., and J. P. Lorimer. 1988. Sonochemistry: Theory, Applications and Uses of Ultrasound in Chemistry. John Wiley & Sons, New York.

Matula, T., I. M. Hallaj, R. O. Cleveland, and L. A. Crum. 1998. The acoustic emissions from single-bubble sonoluminescence. *J. Acoust. Soc. Am*. 103:1377–1382.

Matula, T. J. 1999. Inertial cavitation and single-bubble sonoluminescence. *Phil. Trans. R. Soc. Lond. A*. 357:225–249.

Mayer, R. E., S. Schenk, S. Child, C. Norton, C. Cox, C. Hartman, C. Cox, and E. Carstensen. 1990. Pressure threshold for shock wave induced renal damage. *J. Urol*. 144:1505–1509.

Miller, D., and J. Quddus. 2000. Sonoporation of monolayer cells by diagnostic ultrasound activation of contrast-agent gas bodies. *Ultrasound Med. Biol*. 26:661–667.

Miller, D., A. R. Williams, J. Morris, and W. Chrisler. 1998. Sonoporation of erythrocytes by lithotripter shockwaves in vitro. *Ultrasonics*. 36:947–952.

Miller, M. W., D. L. Miller, and A. A. Brayman. 1996. A review of in vitro bioeffects of inertial ultrasonic from a mechanistic perspective. *Ultrasound Med. Biol*. 22:1131–1154.

Mitragotri, S., D. Edwards, D. Blankschtein, and R. Langer. 1995. A mechanistic study of ultrasonically enhanced transdermal drug delivery. *J. Pharm. Sci*. 84:697–706.

Mitragotri, S., J. Farrell, H. Tang, T. Terahara, J. Kost, and R. Langer. 2000a. Determination of the threshold energy dose for ultrasound-induced transdermal drug delivery. *J. Control. Rel*. 63:41–52.

Mitragotri, S., D. Ray, J. Farrell, H. Tang, B. Yu, J. Kost, D. Blankschtein, and R. Langer. 2000b. Synergistic effect of ultrasound and sodium lauryl sulfate on transdermal drug delivery. *J. Pharm. Sci.* 89:892–900.

Neppiras, E. 1968. Subharmonic and other low frequency emission from bubbles in sound irradiated liquids. *J. Acoust. Soc. Am.* 46:587–601.

Netz, R. R., and M. Schick. 1996. Pore formation and rupture in fluid bilayers. *Phys. Rev. E.* 53:3875–3885.

Ohl, C.-D., T. Kurz, R. Geisler, O. L. Lindau, and W. Lauterborn. 1999. Bubble dynamics, shock waves, and sonoluminescence. *Phil. Trans. R. Soc. Lond. A.* 357:269–294.

Pecha, R., and B. Gompf. 1999. Microimplosions: cavitation collapse and shock wave emission on a nanosecond time scale. *Phys. Rev. Lett.* 84:1328–1330.

Perry, R. H., and D. W. Green. 1973. Chemical Engineering Handbook. McGraw-Hill Book Company, New York.

Prosperetti, A., and Y. Hao. 1999. Modelling of spherical gas bubble oscillations and sonoluminescence. *Phil. Trans. R. Soc. Lond. A.* 357:203–223.

Raeman, C. H., S. Z. Child, D. Dalecki, R. Mayer, K. J. Parker, and E. L. Crstensen. 1994. Damage to murine kidney and intestine from exposure to the fields of a piezoelectric lithotripter. *Ultrasound Med. Biol.* 20:589–594.

Saad, A. H., and G. M. Hahn. 1992. Ultrasound-enhanced effects of adriamycin against murine tumors. *Ultrasound Med. Biol.* 18:715–723.

Shankar, P. M., P. D. Krishna, and V. L. Newhouse. 1999. Subharmonic backscattering from ultrasound contrast agents. *J. Acoust. Soc. Am.* 106:2104–2110.

Sonden, A., B. Svenssin, N. Roman, H. Ostmark, B. Brismar, J. Palmblad, and B. Kjellstrom. 2000. Laser-induced shock wave endothelial cell injury. *Lasers Surg. Med.* 26:364–375.

Stein, W. D. 1986. Diffusion and Transport Across Cell Membranes. Academic Press, Orlando, Florida.

Storey, B. D., and A. J. Szeri. 2000. Water vapor, sonoluminescence and sonochemistry. *Proc. R. Soc. Lond. A.* 456:1685–1709.

Suslick, K. S. 1989. Ultrasound: Its Chemical, Physical and Biological Effects. VCH Publishers, New York.

Tezel, A., A. Sens, and S. Mitragotri. 2002. Investigations of the role of cavitation in low-frequency sonophoresis using acoustic spectroscopy. *J. Pharm. Sci.* 91:444–453.

Tezel, A., A. Sens, J. Tuscherer, and S. Mitragotri. 2001. Frequency dependence of sonophoresis. *Pharm. Res.* 18:1694–1700.

Vichare, N., P. Senthilkumar, V. Moholkar, P. R. Gogate, and A. B. Pandit. 2000. Energy analysis of acoustic cavitation. *Ind. Eng. Chem. Res.* 39:1480–1486.

Wang, Z. Q., R. Pecha, B. Gompf, and W. Eisenmenger. 1999. Single bubble sonoluminiscence: investigations of the emitted pressure wave with a fiber optic probe hydrophone. *Phys. Rev. E.* 59:1777–1780.

Ward, M., and J. Wu. 1999. Ultrasound-induced cell lysis and sonoporation enhanced by contrast agents. *J. Acoust. Soc. Am.* 105:1951–2957.

Ward, M., J. Wu, and J.-F. Chiu. 2000. Experimental study of the effects of optison concentration on sonoporation in vitro. *Ultrasound Med. Biol.* 26:1169–1175.

Weninger, K. R., B. P. Barber, and S. J. Putterman. 1997. Pulsed MIE scattering measurements of the collapse of a sonoluminescencing bubble. *Phys. Rev. Lett.* 78:1799–1802.

Williams, A. R. 1973. A possible alteration in the permeability of ascites cell membranes after exposure to acoustic microstreaming. *J. Cell Sci.* 12:875–885.

Williams, J. C., J. F. Woodward, M. A. Stonehill, and A. P. Evan. 1999. Cell Damage by lithographer shock waves at high pressure to preclude cavitation. *Ultrasound Med. Biol.* 25:1445–1449.

Wu, C. C., and P. H. Roberts. 1993. Shock-wave propagation in a sonoluminescing gas bubble. *Phys. Rev. Lett.* 70:3424–3427.

Wu, J. 2002. Theoretical study on shear stress generated by microstreaming surrounding contrast agents attached to living cells. *Ultrasound Med. Biol.* 28:125–129.

Wu, J., J. P. Ross, and J.-F. Chiu. 2002. Reparable sonoporation generated by microstreaming. *J. Acoust. Soc. Am.* 111:1460–1464.

Zhang, L., L. Cheng, N. Xu, M. Zhao, C. Li, J. Yuan, and S. Jia. 1991. Efficient transformation of tobacco by ultrasonication. *Biotechnology.* 9:996–997.

Zhong, P., I. Ciaonta, S. Zhu, and F. Cocks. 1998. Effects of tissue constraint on shock wave-induced bubble expansion in vitro. *J. Acoust. Soc. Am.* 104:3126–3129.

Zhong, P., H. Lin, and E. Bhogte. 1999. Shock wave-inertial microbubble interaction: methodology, physical characterization, and bioeffect study. *J. Acoust. Soc. Am.* 105:1997–2009.